

# Quadrupole moments and magnetic moments in exotic nuclei

Koichiro Asahi,<sup>\*1,\*2</sup> Hiroshi Ogawa,<sup>\*1,\*2</sup> Hideki Ueno,<sup>\*1</sup> Daisuke Kameda,<sup>\*2</sup> Hisanori Miyoshi,<sup>\*2</sup> Yoshio Kobayashi,<sup>\*1</sup> Akihiro Yoshimi,<sup>\*1</sup> Katsunori Yogo,<sup>\*2</sup> Atsushi Goto,<sup>\*1,\*2</sup> Toshitaka Suga,<sup>\*1,\*2</sup> Kenji Sakai,<sup>\*1,\*2</sup> Nobuaki Imai,<sup>\*3</sup> Yasushi X. Watanabe,<sup>\*1</sup> Ken-ichiro Yoneda,<sup>\*3</sup> Naoki Fukuda,<sup>\*3</sup> Nori Aoi,<sup>\*3</sup> Atsushi Yoshida,<sup>\*3</sup> Toshiaki Kubo,<sup>\*1</sup> Masayasu Ishihara,<sup>\*1</sup> Wolf-Dieter Schmidt-Ott,<sup>\*4</sup> Gerda Neyens,<sup>\*5</sup> and Stephanie Teughels<sup>\*5</sup>

<sup>\*1</sup>*Applied Nuclear Physics Laboratory, RIKEN*

<sup>\*2</sup>*Department of Physics, Tokyo Institute of Technology*

<sup>\*3</sup>*Department of Physics, University of Tokyo*

<sup>\*4</sup>*II. Physikalisches Institut, Universität Göttingen, Germany*

<sup>\*5</sup>*Instituut voor Kern- en Stralingsfysica, University of Leuven, Belgium*

We report on recent results of nuclear moment measurements on exotic nuclei, performed at RIKEN with spin-polarized radioactive nuclear beams. The  $g$ -factor for the  $^{17}\text{C}$  ground state is measured to be  $|g| = 0.5054 \pm 0.0025$ . The obtained value is much smaller than those expected for the lowest  $I^\pi = 1/2^+$  state in shell models and, instead, proves quite compatible with the spin-parity assignment  $I^\pi = 3/2^+$  for the ground state of  $^{17}\text{C}$ . The electric quadrupole moment  $Q$  for  $^{17}\text{B}$  has been measured and found to be surprisingly close to the observed  $Q$  for the neutron shell-closed isotope  $^{13}\text{B}$ . Comparison of the experimental  $Q(^{17}\text{B})$  and  $Q(^{13}\text{B})$  with shell model calculations suggests that the effective charge for neutron is significantly quenched in  $^{17}\text{B}$ , as  $e_n \approx 0.03e$ . Similar analyses have been applied to  $Q(^{15}\text{B})$ ,  $Q(^{14}\text{B})$ , and  $Q(^{18}\text{N})$  obtained in previous experiments. The results clearly indicate the tendency that the effective charge for neutron becomes more and more quenched as the degree of neutron excess increases. The measured magnetic moment for the  $I^\pi = 1/2^+$  ground state of  $^{15}\text{C}$  provides direct information on the value of the spin  $g$ -factor that the neutron acquires when it is embedded in a nucleus. By combining it with the known magnetic moment of  $^{11}\text{Be}$ , we examine the hypothesis that the spin  $g$ -factor for a neutron in a halo state approaches its free-space value.

## Introduction

The domain of nuclei that can be produced in the laboratory for physics experiments has been dramatically expanded recently, thanks to the advances in radioactive nuclear beam (RNB) technology. Systems that are of main concern in nuclear physics are no longer restricted to nuclei at or close to the  $\beta$  stability. The work presented here is intended to make a contribution to such a direction, by taking the spin polarization of RNB as a key experimental grip. The availability of spin-polarized RNBs potentially offers important experimental opportunities in the studies of nuclear structures, fundamental interactions and symmetries,<sup>1)</sup> and other interdisciplinary applications. At present, however, we mainly concentrate on nuclear structure studies via electromagnetic moment measurements.

The electromagnetic moments are one of the basic probes to obtain information about the nuclear structure throughout the entire nuclear chart. The magnetic moment,  $\mu = \langle \psi_{I,M=+I} | \hat{\mu}_z | \psi_{I,M=+I} \rangle$  in terms of the magnetic dipole operator  $\hat{\mu} = \sum_{k=1}^A (g_s \mathbf{s}_k + g_\ell \mathbf{\ell}_k) \mu_N$  and the nuclear magneton  $\mu_N$ , contains weighting factors  $g_s$  and  $g_\ell$  which are very different between the spin  $\mathbf{s}$  and the orbital angular momentum  $\mathbf{\ell}$  ( $g_s = +5.59, g_\ell = +1$  for proton and  $g_s = -3.83, g_\ell = 0$  for neutron, if, for example, bare nucleon values are assumed).

For a given total spin  $I$  where  $\mathbf{I} = \sum_{k=1}^A (\mathbf{s}_k + \mathbf{\ell}_k)$ , the predicted  $\mu$  should differ distinctly for different assumptions on its  $(s, \ell)$  compositions. Thus, under circumstances where the independent particle aspect dominates nuclear motion, the  $\mu$  moment sensitively reflects what single particle orbits contribute to the nuclear wave function. In the other extreme where collective motion plays an important role, the magnetic moment is considered to refer to another characteristic value of  $g$ , i.e.,  $g_R = Z/A$ . Consequently, the magnetic moment may also provide a means to distinguish between spherical and deformed states. One of the interesting cases is found in the Mg and Ne  $N \approx 20$  region where the conventional shell closure for neutron is reported to disappear. In fact, Monte Carlo shell model calculations<sup>2)</sup> predict distinctly small magnetic moments for the first  $2^+$  states in  $^{32}\text{Mg}$ ,  $^{30}\text{Mg}$ , and  $^{28}\text{Ne}$ .

The electric quadrupole moment  $Q$ , representing a deviation from a spherical distribution of the electric charges in a nucleus, is sensitive to the admixture of collective components. In particular, if the valence nucleons are of neutron type, the observation of  $Q$  gives a useful measure of how the core is polarized by the presence of the added particles, since in this case the valence particles themselves are neutral and should not directly contribute to the *electric* quadrupole moment.

In what follows, we first outline two key ingredients of

moment measurements at the RIKEN RNB facility, i.e., an element-independent production of nuclear polarization through the projectile fragmentation (PF) process, and an ultra-sensitive detection of nuclear magnetic resonance via the  $\beta$ -ray asymmetry. Then, we present the results obtained for the  $g$ -factor of the ground state of  $^{17}\text{C}$  and discuss the assignment of its spin. In the succeeding section, we focus on the  $Q$  moment results, in which an interesting phenomenon of quenching of the E2 effective charge in neutron-rich nuclei is implied. Finally, a discussion is made on the possibility of restoration of free nucleon moment in the halo state, based on the recent magnetic moment results for  $^{15}\text{C}$ .

## Experimental methods

### Production of spin-polarized RNBs

There are two major approaches to obtain beams of radioactive nuclei. The first one is based on the production of radioactive nuclei via the target fragmentation (TF) reaction induced by a high-energy proton beam, taking advantage of high available beam intensities for protons and thick adoptable targets. The activities produced come immediately to rest in the target, diffuse out, are ionized, and then are accelerated to form a beam that is then mass-separated in a magnet of an isotope separator on line (ISOL). The other approach for RNB production, the PF method, relies on the fragmentation of beam particles. Heavy ion beams at several tens of MeV/u or higher are used. The activities, projectile fragments, are produced almost at rest in the projectile-rest frame, or as a beam well focused in angle and velocity in the laboratory frame. The fragment beam thus obtained is immediately delivered to an in-flight isotope separation by means of combined magnetic-rigidity and momentum-loss analyses. The latter method using the PF reaction is rather new compared to the former (TF-ISOL method) that has been well developed at ISOLDE/CERN. Because of the fast, chemistry-independent nature of the in-flight isotope separation mechanism, the PF method applies to quite wide regions of nuclei without the need for elaborate technical developments. For this reason, it may be considered that RNB physics largely owes its recent progress to the advent of the PF method.

The momentum distribution of projectile fragments in the PF reaction is characterized by a sharp, Gaussian-like peak located around the beam velocity, and is fairly well explained in terms of a simple participant-spectator model.<sup>3)</sup> In this model, the collision between a projectile and a target nucleus is considered as a simple ensemble of independent collisions between individual nucleons in the projectile and those in the target. Nucleons in a part of projectile volume that overlaps with the target at collision are removed from the projectile as illustrated in Fig. 1, leaving the remaining portion (projectile fragment) in its original motion. The fragment momentum then is given by  $\vec{p} = M\vec{v}_0 - \vec{p}_r$ , where  $M$  and  $\vec{v}_0$  denote the fragment mass and the projectile velocity, respectively.  $\vec{p}_r$  is the internal momentum of the nucleon(s) removed from the projectile. Noting that the angular momentum,  $\vec{L}_r = \vec{R} \times \vec{p}_r$  (with  $\vec{R}$  representing the c.m. position of the removed nucleons measured from the projectile center), accompanies the removed nucleons, one may be led to an expectation that the fragment spin, given by  $\vec{L} = -\vec{L}_r$ , is correlated with the linear momentum  $\vec{p}$ , and thus the fragment will be spin-polarized by simply selecting its linear momentum. An experiment to examine this expectation was performed by us for the fragmentation of  $^{14}\text{N}$  projectile at 40 MeV/u on an Au target.<sup>4)</sup>

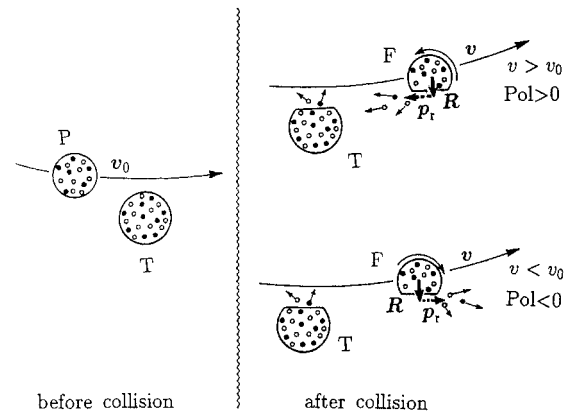


Fig. 1. Predicted correlation between fragment spin and linear momentum in a model of projectile fragmentation. Projectile P incident at velocity  $v_0$  is transmuted to fragment F through the removal of nucleons at position  $\vec{R}$ . See text for further explanation.

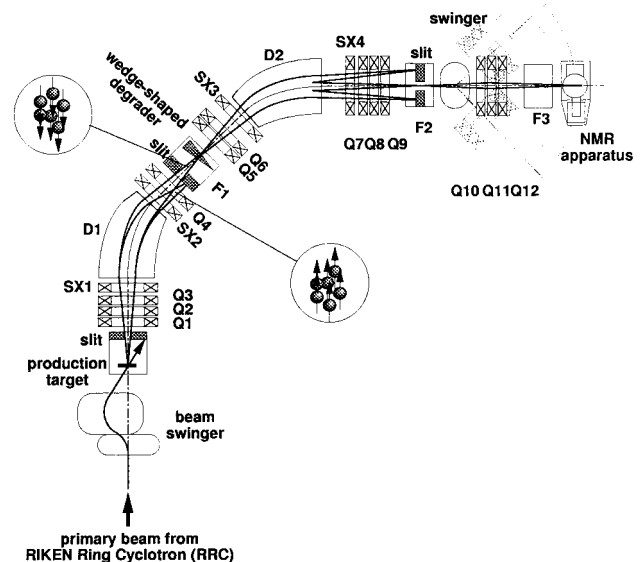


Fig. 2. Arrangement of the beam line RIPS for the production of spin-polarized radioactive nuclear beams at RIKEN.

The data indeed revealed a substantial polarization of  $^{12}\text{B}$  fragments with the momentum dependence compatible with the expectation from the above simple model. Subsequent experiments since then<sup>5-7)</sup> have shown that the polarization is a general phenomenon common to fragmentation reactions. The size of polarization obtained in this method typically ranges from 2 to 10%.

### $\beta$ -NMR technique

A typical arrangement for nuclear moment measurements with polarized RNBs at RIKEN is shown in Fig. 2. A primary beam of energies around  $E/A = 100$  MeV/u from the RIKEN Ring Cyclotron is introduced into a target chamber through a beam swinger, so that fragments emitted from the target at finite angles are accepted by the fragment separator RIPS.<sup>8)</sup> Fragments of the objective nuclide are isotope-separated and momentum-analyzed in RIPS, and finally focused on a collection point F3, at which a stopping material and a device

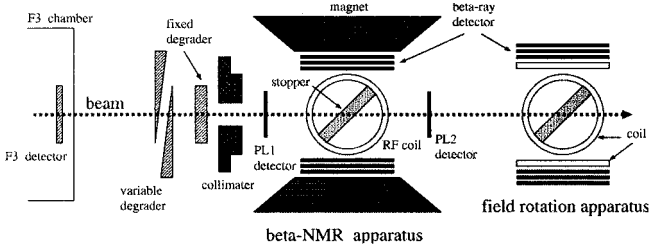


Fig. 3. Setup at the collection point F3 of the RIPS beam line, for moment measurements with polarized RNBs.

for  $\beta$ -ray detected nuclear magnetic resonance ( $\beta$ -NMR) experiments are located. The setup at F3 for the  $\beta$ -NMR experiments is schematically shown in Fig. 3. The polarization of fragments in the direction perpendicular to the reaction plane (referred to as the  $z$ -direction below) is preserved during the transportation through RIPS to the stopper, and held in the stopper under an applied static magnetic field  $B_0$  in the  $z$ -direction until the fragments decay due to the  $\beta$ -ray emission. The  $\beta$ -ray angular distribution from polarized nuclei is given by  $W(\theta) = 1 + \frac{v}{c} A_\beta P \cos \theta$ , where  $A_\beta$  and  $P$  denote the asymmetry parameter and the degree of polarization, respectively, and  $v/c \approx 1$  is the ratio of the  $\beta$  particle velocity to the speed of light. A change in the up/down ratio  $U/D \equiv W(0^\circ)/W(180^\circ) \approx 1 + 2A_\beta P$  of the  $\beta$ -ray intensities provides a sensitive index for the spin flip resulting from the nuclear magnetic resonance (NMR). An rf field  $B_1$  perpendicular to  $B_0$  is applied, with its frequency  $\nu$  being swept over the range from  $\nu_1 - \frac{1}{2}\Delta\nu$  to  $\nu_1 + \frac{1}{2}\Delta\nu$ . If the range includes the Larmor frequency  $\nu_L = \mu B_0/hI$ , the nuclear spins are inverted (the adiabatic fast passage inversion; AFP) and the  $U/D$  ratio changes as  $1 + 2A_\beta P \rightarrow 1 - 2A_\beta P$ . Thus, the NMR is searched for by scanning the  $\nu_1$  value while monitoring the  $\beta$ -ray  $U/D$  ratio.

Once the NMR is successfully detected, the degree of polarization  $P$  for the fragment beam can be deduced from the observed size of change in asymmetry. In order to pursue the NMR search, however, it is highly desirable to know  $P$  before the NMR effect is found, since the sensitivity of the search depends on the size of  $P$ . This situation represents a dilemma inherent in the present “ $\beta$ -NMR on fragmentation-induced polarization” experiment. Recently, we have developed a means to overcome this dilemma: The degree of polarization for fragments is measured prior to the NMR search by means of the adiabatic field rotation technique.<sup>9)</sup> Using this technique, the best experimental conditions are searched for by changing the settings for the emission angle  $\theta_L$  and the momentum  $p$ , in order to optimize the figure of merit given by  $F = P^2 Y$ , where  $Y$  is the yield for the objective fragments.

In the measurement of electric quadrupole moment  $Q$ , a single crystal stopper is employed, in which an electric field gradient  $eq$  is known to act on an implanted radioactive atom. In the spin  $I = 3/2$  case, the quadrupole coupling between  $eq$  and  $Q$  causes the NMR line to split into three frequencies  $\nu = \nu_L, \nu_L \pm \frac{3}{8}\nu_Q$ , where  $\nu_Q \equiv eqQ/h$ . The measurement is made by applying the  $B_1$  field having all of the three frequency components with the  $\nu_Q$  value being scanned.

The above method of “ $\beta$ -NMR on fragmentation-induced polarization” has been applied to the measurement of mag-

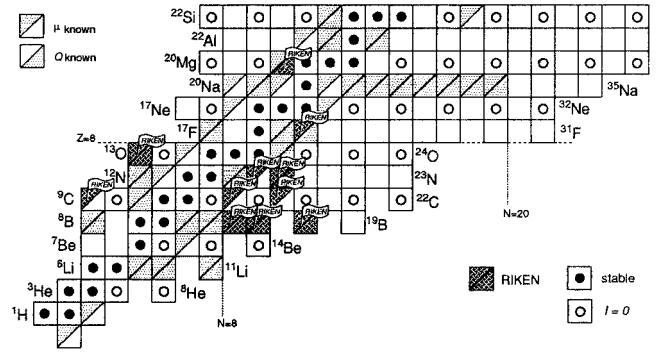


Fig. 4. Nuclides for which the magnetic moments or the electric quadrupole moments have been determined.

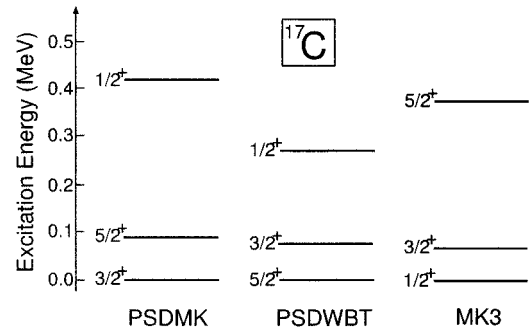


Fig. 5. Low-lying levels in  $^{17}\text{C}$  from shell model calculations. Those with PSDMK and PSDWBT interactions are calculated using OXBASH code, while that with MK3 interaction is taken from Ref. 10.

netic dipole and electric quadrupole moments for numbers of nuclei situated in the light-mass, neutron-rich region. In Fig. 4, we show nuclides for which the magnetic dipole or the electric quadrupole moments are determined at RIKEN. To date, ten new magnetic dipole moments and six new electric quadrupole moments have been determined. Here we discuss the physical implications of some of the results of these experiments.

#### $g$ -factor for the $^{17}\text{C}$ ground state and its spin value

The spin for the ground state of  $^{17}\text{C}$  is not known. In shell models, there appear three low-lying states with  $I^\pi = 1/2^+, 3/2^+$ , and  $5/2^+$ , which are very close to each other, and which state has the lowest energy depends critically on the interaction employed in the calculation, as seen in Fig. 5. This situation makes it very difficult to predict the spin for the  $^{17}\text{C}$  ground state from theory. Experimentally, one of the candidates,  $I^\pi = 5/2^+$ , is excluded from the observed branching ratios for the  $^{17}\text{C} \rightarrow ^{17}\text{N}$   $\beta$  decay,<sup>10)</sup> but the other two,  $I^\pi = 1/2^+$  and  $3/2^+$ , remain intact. The spin assignment for the  $^{17}\text{C}$  ground state is quite crucial in interpreting the results of single-neutron removal reaction.<sup>11–14)</sup> The longitudinal momentum distribution of the outgoing  $^{16}\text{C}$  fragments in this reaction reflects the  $\ell$  value that the removed neutron possesses initially in  $^{17}\text{C}$ . In the case of the  $s_{1/2}$  orbit for the valence neutron, a narrow longitudinal momentum distribution is expected because of its small binding energy

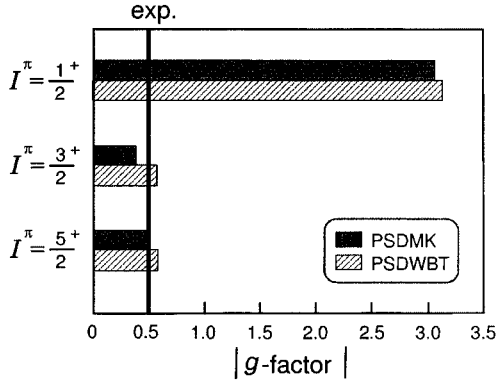


Fig. 6. Theoretical and experimental  $g$ -factors for the  $^{17}\text{C}$  ground state.

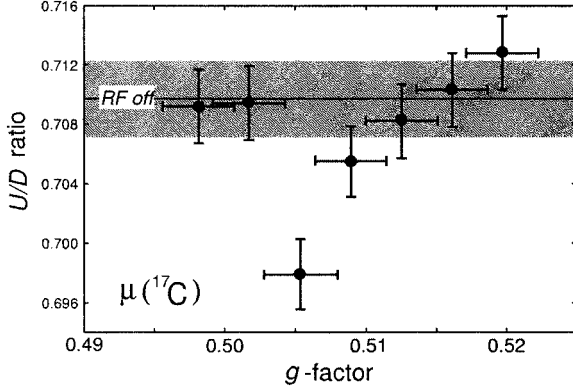


Fig. 7.  $\beta$ -NMR spectrum for the measurement of  $g$ -factor for the  $^{17}\text{C}$  ground state.

( $S_n \approx 0.73$  MeV). The experimental distribution is reported to be much broader favoring the  $d$  orbit, but the shape of the spectrum does not conform to the pure  $d$  state. More recently, spectroscopic factors and  $\ell$  assignments have been derived from measured partial cross sections and associated momentum distributions corresponding to the  $^{16}\text{C}$  final states.

In the present work, the  $g$ -factor for the  $^{17}\text{C}$  ground state has been determined. The  $g$  measurement is very important in distinguishing between the two spin-parity assignments  $I^\pi = 1/2^+$  and  $3/2^+$ . For the former case of assignment, the angular momentum  $I = 1/2$  is considered to stem almost solely from the neutron spin, since only configuration of  $^{16}\text{C}(0^+) \otimes \nu s_{1/2}$  type is possible within the  $(\nu d_{5/2} s_{1/2})^3$  space. Then the  $g$ -factor for  $^{17}\text{C}$  should take a large value close to  $g_n = -3.83$ . For the latter case, on the other hand, the major configurations would be of  $\nu(d_{5/2})^3$  and  $[\nu(d_{5/2})^2 s_{1/2}]$  types, both giving  $g$ -values  $1/5$  times of  $g_n$  or even smaller. In fact, shell-model calculations for the low-lying states in  $^{17}\text{C}$  using PSDMK and PSDWBT interactions with the free M1 operator, shown in Fig. 6, show a clear difference in  $g$  for the  $I^\pi = 1/2^+$  and  $3/2^+$  assignments. The theoretical  $g$ -values do not depend much on the choice of the M1 operator. For instance, employing the effective M1 operator from the work of Arima *et al.*<sup>15)</sup> for proton and that from Brown and Wildenthal<sup>16)</sup> for neutron leads to a  $I^\pi = 1/2^+$  state  $g$ -factor that is only 10 % smaller than that with the free M1 operator.

A spin-polarized beam of  $^{17}\text{C}$  was produced in the frag-

## Effective Charges

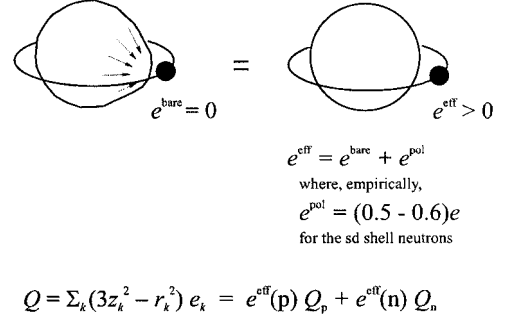


Fig. 8. Effective charge for neutron.

mentation of  $^{22}\text{Ne}$  projectiles on an  $^{93}\text{Nb}$  target at  $E/A = 110$  MeV/u. The  $^{17}\text{C}$  fragments were implanted in a Pt stopper cooled at about 75 K. The  $\beta$ -NMR spectrum obtained is plotted in Fig. 7. From the frequency corresponding to a dip in the spectrum, we tentatively deduce the  $g$ -factor for the  $^{17}\text{C}$  ground state:  $|g(^{17}\text{C})| = 0.5054 \pm 0.0025$ . The obtained  $|g(^{17}\text{C})|$  is much smaller than the theoretical  $g$  for the  $1/2^+$  state plotted in Fig. 6 and, on the contrary, shows good agreement with that for the  $3/2^+$  assignment. We thus clearly conclude the spin-parity assignment for the ground state of  $^{17}\text{C}$  as  $I^\pi = 3/2^+$ . We find that in the wave function for the  $I^\pi = 3/2^+$  state obtained from the calculations presented in Fig. 6, the configurations of types  $\nu(d_{5/2})^3$  and  $[\nu(d_{5/2})^2 s_{1/2}]$  share almost equal strengths.

## Quenching of effective charges in neutron-rich nuclei

We now focus on the quadrupole moment results. The nuclear electric quadrupole moment is written as  $Q = \langle \psi_{I,M=+I} | \sum_{k=1}^A e_k \hat{Q}_k | \psi_{I,M=+I} \rangle$ , where  $\hat{Q}_k = \sqrt{\frac{16\pi}{5}} r_k^2 Y_{20}(\hat{r}_k)$  and  $e_k$  is the electric charge for the  $k$ -th nucleon. Since  $e_k = 0$  for neutron, there should appear no direct contribution from neutrons; however, this point requires further attention: The addition of a valence neutron will induce polarization of the core into configurations outside the adopted model space. Such an effect is included by introducing effective charges  $e_p^{\text{eff}} = e + \delta e_p$  and  $e_n^{\text{eff}} = \delta e_n$  for proton and neutron, as illustrated in Fig. 8. Empirically, the polarization charges are known to take values  $\delta e_p \approx 0.29e$  and  $\delta e_n \approx 0.49e$  for nuclei in the region close to stability with mass range  $A = 17$ –39. It is interesting to examine how such a property of nucleon in a nucleus changes as it moves farther from stability.

The electric quadrupole moment for the  $^{18}\text{N}$  ground state has been measured<sup>17)</sup> to be  $|Q(^{18}\text{N})| = 12.3 \pm 1.2$  emb. Because of the  $p_{1/2}$  character of an  $^{18}\text{N}$  proton hole, the proton contribution to the  $Q$  moment is very small: Rewriting as  $Q = e_p^{\text{eff}} Q_p + e_n^{\text{eff}} Q_n$  where  $Q_p = \langle \psi_{I,+I} | \sum_{\text{proton}} \hat{Q}_k | \psi_{I,+I} \rangle$  and  $Q_n = \langle \psi_{I,+I} | \sum_{\text{neutron}} \hat{Q}_k | \psi_{I,+I} \rangle$ , shell model calculations with the PSDMK and PSDWBT interactions predict  $Q_p = 1.7$ –2.0 mb while  $Q_n = 31.8$ –33.4 mb. Note that the calculated  $Q_{p,n}$  values are quite stable against the choice of the effective interaction. Inserting the usually taken values of effective charges,  $e_p^{\text{eff}} \approx 1.3e$  and  $e_n^{\text{eff}} \approx 0.5e$ , the shell model

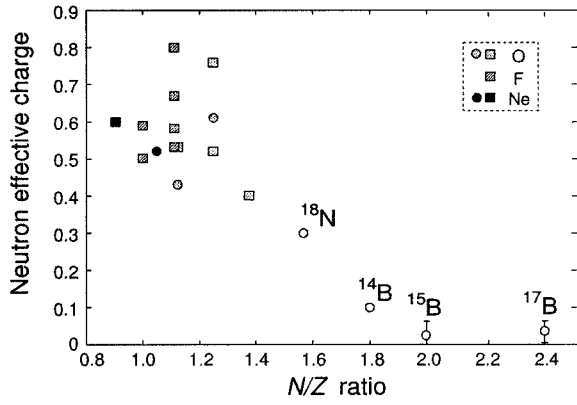


Fig. 9. Empirical effective charge for neutrons in the  $sd$  orbits, extracted from the experimental static  $Q$  moments (circles) and E2 transition probabilities (boxes).

values for  $Q$  substantially overestimate the experimental  $Q$ . Because  $Q_p$  is very small, the small  $Q(^{18}\text{N})$  implies that  $e_n^{\text{eff}}$  should be smaller. Agreement is obtained if  $e_n^{\text{eff}} = 0.3e$  is taken.

The quenching of  $e_n^{\text{eff}}$  is even more striking in the measured  $Q$  moments for  $^{15}\text{B}$ <sup>18)</sup> and  $^{17}\text{B}$ <sup>19)</sup>. The  $^{15}\text{B}$  and  $^{17}\text{B}$  isotopes have, respectively, two and four extra neutrons on top of the closed-shell  $N = 8$  isotope  $^{13}\text{B}$ . Shell model calculations predict a rapid increase of the matter  $Q$  moment for neutrons  $Q_n$  from 0.0 mb through 45.3 mb to 60.5 mb<sup>\*1</sup> for isotopes  $^{13}\text{B}$ ,  $^{15}\text{B}$ , and  $^{17}\text{B}$ , respectively, while that for proton stays almost constant,  $Q_p = 31.2\text{--}25.1$  mb. Thus, the shell model values for  $Q$  increases by about 40% and 55% as going from  $^{13}\text{B}$  to  $^{15}\text{B}$  and  $^{17}\text{B}$  isotopes, if the standard value of  $e_n^{\text{eff}} \approx 0.5e$  is assumed for the neutron effective charge. To the contrary, the experimental  $Q$  moments,  $|Q(^{15}\text{B})| = 38.01 \pm 1.08$  emb<sup>18)</sup> and  $|Q(^{17}\text{B})| = 38.8 \pm 1.5$  emb (preliminary),<sup>19)</sup> are surprisingly close to that of  $^{13}\text{B}$ ,  $|Q(^{13}\text{B})| = 36.9 \pm 1.0$  emb.<sup>20, 21)</sup><sup>\*2</sup> In a weak coupling model in which  $^{15}\text{B}$  and  $^{17}\text{B}$  are described by two and four neutrons coupled to the  $^{13}\text{B}$  core, the similarities of  $Q(^{15}\text{B})$  and  $Q(^{17}\text{B})$  to  $Q(^{13}\text{B})$  imply smallness of the neutron part of  $Q$  in  $^{15}\text{B}$  and  $^{17}\text{B}$ . Therefore, it may be interesting to assume that the effective charge for neutron is quenched while that for proton remains unaltered, although other possibilities cannot be excluded. To obtain agreement between theory and experiment under this assumption, anomalously small values for the neutron effective charge,  $e_n^{\text{eff}} \leq 0.1e$ , are needed. The experimental  $Q$  of  $^{14}\text{B}$ ,  $|Q(^{14}\text{B})| = 29.84 \pm 0.75$  emb,<sup>18)</sup> is found to be well reproduced by calculations with  $e_n^{\text{eff}} \approx 0.1e$ . The  $e_n^{\text{eff}}$  values extracted from the present experiments are plotted in Fig. 9 as a function of the  $N/Z$  ratio, together with those for nuclei close to stability taken from literature. One may find an apparent tendency that the quenching of  $e_n^{\text{eff}}$  develops gradually as  $N/Z$  increases.<sup>22)</sup>

\*1 Values from calculations with the PSDMK interaction. We stress again that the calculated  $Q$  is very stable against the choice of the effective interactions, and therefore the discrepancy observed here is substantial.

\*2 Re-evaluated from  $Q(^{13}\text{B})$  reported in Ref. 20 (which takes the old data for  $Q(^{12}\text{B})$  as a reference) by taking the new  $Q(^{12}\text{B})$  value from Ref. 21 as a reference.

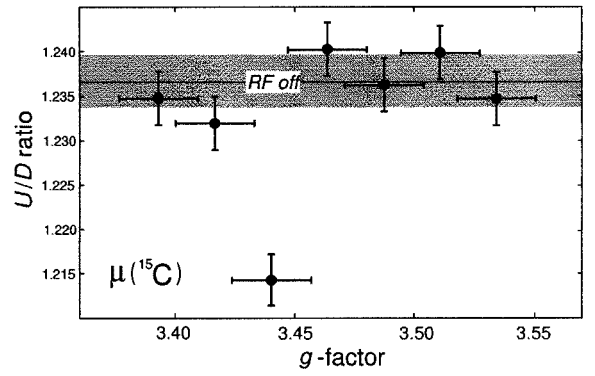


Fig. 10.  $\beta$ -NMR spectrum obtained for the measurement of  $g$ -factor for the ground state of  $^{15}\text{C}$ .

Does the magnetic moment of halo nucleon tend to recover its free space value?

The ground state of  $^{11}\text{Be}$ , with its anomalous spin-parity  $I^\pi = 1/2^+$  and small neutron separation energy  $S_n = 503$  keV, is known to have a one-neutron halo structure. Then, an interesting question arises whether the spin  $g$ -factor for a neutron in a halo,  $g_s^{\text{eff}}(\text{halo})$ , tends to recover the free nucleon value, since a halo neutron is considered to spend most of its time in space outside the nucleus. The  $g_s^{\text{eff}}(\text{halo})$  may be extracted from an observed  $^{11}\text{Be}_{\text{g.s.}}$  magnetic moment. More quantitatively, in a weak coupling model, the  $^{11}\text{Be}_{\text{g.s.}}$  wave function is expressed as  $|^{11}\text{Be}_{\text{g.s.}}(1/2^+)\rangle = \alpha|^{10}\text{Be}(0^+) \otimes \nu s_{1/2}\rangle^{J^\pi=1/2^+} + \beta|^{10}\text{Be}(2^+) \otimes \nu d_{5/2}\rangle^{J^\pi=1/2^+}$ , where  $\alpha^2 \approx 0.55$  is predicted by the variational shell model.<sup>23)</sup> The  $^{11}\text{Be}_{\text{g.s.}}$  magnetic moment is then given by Ref. 23, 24

$$\mu(^{11}\text{Be}_{\text{g.s.}}) = \alpha^2 \mu(\nu s_{1/2}) + (1 - \alpha^2) \left[ \frac{7}{15} \mu(\nu d_{5/2}) - \frac{1}{3} \mu(2^+) \right]. \quad (1)$$

The  $\mu(^{11}\text{Be}_{\text{g.s.}})$  is experimentally known<sup>25)</sup> to be  $\mu(^{11}\text{Be}_{\text{g.s.}}) = -1.6816 \pm 0.0008 \mu_N$ , while the  $^{10}\text{Be}(2^+)$  core moment  $\mu(2^+)$  is evaluated as  $\mu(2^+) = 1.786 \mu_N$  in Ref. 26 from the shell-model wave function. The  $d_{5/2}$  neutron moment  $\mu(\nu d_{5/2})$  is expressed as  $\mu(\nu d_{5/2}) = \frac{1}{2} g_s^{\text{eff}} \mu_N$ , in terms of the effective spin  $g$ -factor  $g_s^{\text{eff}}$  for (non-halo) neutron inside a nucleus. Thus, if the (non-halo) neutron  $g_s^{\text{eff}}$  factor is known, we obtain the  $g_s$ -factor for the halo  $s_{1/2}$  state neutron through Eq. (1).

$\beta$ -NMR measurement of the  $^{15}\text{C}_{\text{g.s.}}$  magnetic moment was carried out. The result is shown in Fig. 10. A preliminary analysis of the data gives  $|\mu(^{15}\text{C})| = (1.720 \pm 0.009) \mu_N$ .<sup>19)</sup> Shell-model calculations indicate that the  $^{15}\text{C}_{\text{g.s.}}$  wave function is dominated by configurations of  $\pi(0^+) \otimes \nu s_{1/2}$  to 97–98% probability. After correction for the remaining 2–3% contribution from the other types of configurations, we obtain the “experimental”  $2s_{1/2}$  neutron single particle moment,  $\mu(\nu s_{1/2})^{\text{exp}} = -(1.77 \pm 0.05) \mu_N$ , or the effective  $g_s$ -factor for well-bound (i.e., non-halo) neutron,  $g_s^{\text{eff}} = (0.92 \pm 0.02) g_s^{\text{bare}}$ , where  $g_s^{\text{bare}} = -3.83$  is the free-neutron  $g$  factor.

By inserting  $g_s^{\text{eff}}$  into Eq. (1), the  $g_s$  value for the halo neutron is obtained. Interestingly,  $g_s^{\text{eff}}(\text{halo}) \approx 0.99 g_s^{\text{bare}}$  is obtained if we employ  $\alpha^2 \approx 0.55$  predicted by VSM, as indicated in Fig. 11. On the other hand, if a larger value of  $\alpha^2 \approx 0.84$

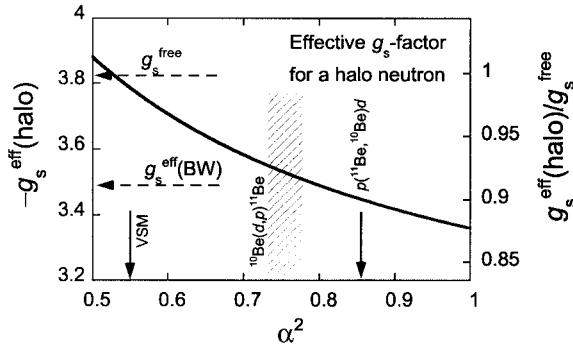


Fig. 11. Halo-neutron  $g_s$ -factor derived from the experimental  $g$ 's for  $^{11}\text{Be}$  and  $^{15}\text{C}$ , as a function of  $\alpha^2$ .

derived from  $p(^{11}\text{Be},^{10}\text{Be})d$  reaction<sup>27)</sup> is employed, an almost normal value of  $g_s^{\text{eff}}(\text{halo}) \approx 0.90g_s^{\text{bare}}$  is obtained. Thus, further studies are needed to solve the present problem.

#### References

- 1) K. Sugimoto, M. Ishihara, and N. Takahashi: in *Treatise on Heavy-Ion Science* Vol. 3, edited by A. Bromley (Plenum Publ., New York, 1985), p.397.
- 2) T. Otsuka et al.: Nucl. Phys. A **682**, 155c (2001).
- 3) A. S. Goldhaber: Phys. Lett. B **53**, 306 (1974).
- 4) K. Asahi et al.: Phys. Lett. B **251**, 488 (1990).
- 5) K. Asahi et al.: Hyperfine Interact. **75**, 101 (1992).
- 6) H. Okuno et al.: Hyperfine Interact. **78**, 97 (1993).
- 7) H. Okuno et al.: Phys. Lett. B **335**, 29 (1994).
- 8) T. Kubo: Nucl. Instrum. Methods Phys. Res. B **70**, 309 (1992).
- 9) H. Ogawa et al.: in preparation.
- 10) E. K. Warburton and D. J. Millener: Phys. Rev. C **39**, 1120 (1989).
- 11) T. Baumann et al.: Phys. Rev. Lett. **439**, 256 (1998).
- 12) D. Bazin et al.: Phys. Rev. C **57**, 2156 (1998).
- 13) E. Sauvan et al.: Phys. Lett. B **491**, 1 (2000).
- 14) V. Maddelena et al.: Phys. Rev. C **63**, 024613 (2001).
- 15) A. Arima, K. Shimizu, W. Bentz, and H. Hyuga: Adv. Nucl. Phys. **18**, 1 (1987).
- 16) B. A. Brown and B. H. Wildenthal: Nucl. Phys. A **474**, 290 (1987).
- 17) H. Ogawa et al.: Phys. Lett. B **451**, 11 (1999).
- 18) H. Izumi et al.: Phys. Lett. B **366**, 51 (1996).
- 19) H. Ogawa et al.: Proc. RIKEN Symp. Shell Model 2000, Wako, 2000-3, to appear in Nucl. Phys. A (2001).
- 20) R. C. Haskell and L. Madansky: J. Phys. Soc. Jpn. **34** Suppl., 167 (1973).
- 21) T. Minamisono et al.: Phys. Rev. Lett. **69**, 2058 (1992).
- 22) H. Sagawa and K. Asahi: Phys. Rev. C **63**, 064310 (2001).
- 23) T. Otsuka et al.: Phys. Rev. Lett. **70**, 1385 (1993).
- 24) T. Suzuki and T. Otsuka: Proc. RIKEN Symp. Shell Model 2000, Wako, 2000-3, to appear in Nucl. Phys. A (2001).
- 25) W. Geithner et al.: Phys. Rev. Lett. **83**, 3792 (1999).
- 26) T. Suzuki et al.: Phys. Lett. B **364**, 69 (1995).
- 27) S. Fortier et al.: Phys. Lett. B **461**, 22 (1999).